Dynamics and critical damping of capillary waves in an ionic liquid

E. Sloutskin,[1] P. Huber,[2] M. Wolff,[2] B. M. Ocko,[3] A. Madsen,[4] M. Sprung,[5] V. Schön,[2] J. Baumert,[3,*] and M. Deutsch[1,†]

[1]*Physics Department and Institute of Nanotechnology and Advanced Materials, Bar-Ilan University, Ramat-Gan 52900, Israel*
[2]*Department of Physics and Mechatronics Engineering, Saarland University, Saarbrücken, Germany*
[3]*Condensed Matter Physics & Materials Sciences Department, Brookhaven National Laboratory, Upton, New York 11973, USA*
[4]*European Synchrotron Radiation Facility, B.P. 220, F-38043 Grenoble, France*
[5]*APS, Argonne National Laboratory, Argonne, Illinois 60439, USA*

The dynamics of thermal capillary waves (CWs) on an ionic liquid's surface are studied at the transition from propagating to overdamped CWs by x-ray photon correlation spectroscopy. The analysis considers both homodyne and heterodyne contributions, and yields excellent full line-shape experiment-theory agreement for the structure factor. The CWs' Brillouin scattering becomes extinct at a critical temperature $T_c^{JK} \sim 10$ K above T_c^{LL}, the propagating modes' hydrodynamic limit, in agreement with linear response theory. Surprisingly, the same power law applies at both T_c. The results rule out the presence of a suggested surface dipole layer.

Synthesized first in 1914 [1], room-temperature ionic liquids (RTILs), organic salts with room-temperature melting points, have been intensely studied over the last decade for numerous applications such as "green" solvents in chemical synthesis [2], batteries [3], fuel and solar cells [4], and even telescope construction [5]. Their great interest to basic science is due to their peculiar molecular structure and composition (a bulky organic cation with a small inorganic anion), which produce unusual molecular packings, and to a complex combination of interactions (van der Waals, ionic, dipolar, and hydrogen bonding) seldom occurring together in other materials [6]. Among over a thousand RTILs synthesized to date, 1-butyl-3-methylimidazolium tetrafluoroborate ([bmim][BF$_4$]) is one of the best studied [7–10] due to its favorable physicochemical properties for many applications [9,11]. It is also one of the only two RTILs for which the *static* structure of the free surface has been measured with submolecular resolution [8,12], including, in particular, the time-averaged contribution from thermally excited capillary waves (CWs), present at all liquid interfaces [13,14]. However, time-resolved CW *dynamics* measurements by grazing-incidence x rays, which sample the surface to a small ~ 50 Å depth only, are not available for any RTIL. X-ray photon correlation spectroscopy (XPCS) is a method of choice for such studies. The time (τ) correlations of CW-scattered photons, $G(q_x, \tau)$ (arguments defined in Fig. 1), yield the CW spectrum, $S(k, \omega)$ (k, ω being the CW wave vector and angular frequency), and its Fourier transform, the dynamic surface height-height correlation function, $C(k, \tau)$, the physical quantity of interest.

We report here XPCS measurements for [bmim][BF$_4$], which was chosen for its air and temperature stability, availability with high purity [8,9], and its known physicochemical properties. Recent x-ray reflectivity measurements [8] show that [bmim][BF$_4$] has a dense, 6-Å-thick layer at its free surface, which may influence the surface dynamics, as do Langmuir films [15,16] and surface-frozen layers [17]. Dy-

namic light-scattering (DLS) measurements of a related RTIL suggested the existence of a dipole layer at the surface exhibiting a ferroelectric order-disorder transition with temperature [18]. Also, [bmim][BF$_4$] should exhibit a transition from propagating to overdamped CWs. The pioneering, and only, XPCS study of such a transition [19] in a water-glycerol mixture, lacked independently measured surface tension and viscosity values, and employed a simplified analysis, as discussed below.

Undulators at third-generation synchrotrons deliver coherent beams of sufficient intensity for XPCS measurements on liquid surfaces [19–22]. The use of grazing incidence and short wavelength ($\lambda = 1.54481$ Å) has several advantages over DLS, among them surface specificity and the ability to probe much shorter length scales [20,23,24]. In DLS, the scattered light is mixed with a coherent reference beam, producing a heterodyne (rather than a homodyne) signal, which provides field (rather than intensity) correlation information. In XPCS, spontaneous heterodyning occurs [20], tentatively
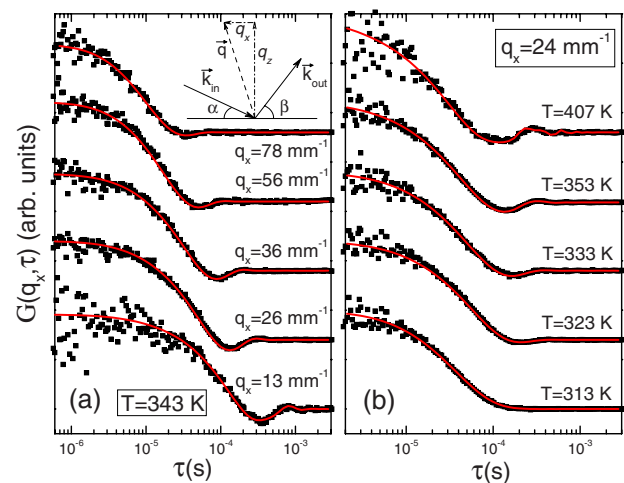

FIG. 1. (Color online) Measured (symbols) and theory-fitted (lines) time-correlation functions at the listed q_x (a) and T (b), y shifted for clarity. Inset: The scattering geometry. k_{in}, k_{out}, q_z, q_x, and q are the incoming and outgoing wave vectors and the surface-normal, -parallel, and total wave vector transfers.

---

*Deceased.

†deutsch@mail.biu.ac.il

assigned to the breakdown of the Fraunhofer conditions [20,21]. Moreover, both homodyne and heterodyne signals may be present. We show below that a quantitative analysis of the measured data is still possible, even without knowing what causes the spontaneous heterodyning.

Measurements were done at ID10A Troïka I beamline, ESRF (Grenoble, France), at a grazing incidence angle $\alpha = 0.114°$, slightly below the critical angle for total reflection. Samples, obtained from Chemada Ltd. and purified as discussed elsewhere [8], were placed in an evacuated, temperature-controlled cell. A fast avalanche photodiode detector and a Flex01-08D correlator were used. To obtain a surface-parallel wave vector transfer, $q_x = (2\pi/\lambda)(\cos\alpha - \cos\beta)$, the detector was placed at a non-specular angle $\beta \neq \alpha$ within the reflection plane [Fig. 1(a), inset], and measured time correlations for the diffusely scattered radiation. The incident beam pinhole was 10 μm × 10 μm. The detector slit [25–50 μm(w) × 10 μm (h), 1250 mm from the sample] provided a pointlike ($\pm 3 \times 10^{-8}$ Å^{-1}) q_x resolution, but a coarse [$\pm (4-8) \times 10^{-5}$ Å^{-1}] q_y resolution, requiring integration over a rectangular resolution function throughout our analysis to avoid an erroneous interpretation of the measurements [25].

Figure 1 shows the measured and background-subtracted XPCS spectra. All curves in Fig. 1(a) exhibit decaying oscillations, the signature of propagating CWs. The CWs' frequency is roughly inversely proportional to the dip position, implying an almost linear dispersion relation. By contrast, the $T = 313$ K curve in Fig. 1(b) decays exponentially, showing viscosity-overdamped CWs at this T. The viscosity's exponential T dependence increases the damping as T decreases. So does an increase in q_x, since the fluid's viscous dissipation depends on spatial gradients in the velocity [26] and these are larger for shorter wavelengths.

To obtain a theoretical expression for fitting the measured $G(q_x, \tau)$, we first address the CW modes allowed by hydrodynamics, though not necessarily excited in a particular system, then discuss the actual modes thermally excited in our system. The hydrodynamic modes obey the linearized Navier-Stokes equation, subject to surface boundary and liquid continuity conditions [16,27]. Levich and Lucassen-Reynders and Lucassen (LL) obtain the dispersion relation, $D(k, \tilde\omega) = 0$ [16],

$$D(k, \tilde\omega) \equiv gk + \gamma k^3/\rho - \tilde\omega^2 - i\tilde\omega\Gamma(k, \tilde\omega) = 0, \quad (1)$$

where $g = 9.8$ m/s^2, γ, $\nu = \eta(T)/\rho(T)$, η, and ρ are, respectively, the gravitational acceleration, surface tension, kinematic and static viscosities, and density. $\Gamma(k, \tilde\omega) = 4\varepsilon + 4i\varepsilon^2/\tilde\omega[1 - \sqrt{1 - i\tilde\omega/\varepsilon}]$, where $\varepsilon = \nu k^2$. The roots of Eq. (1) (obtained numerically) are the CWs' complex angular frequencies, $\tilde\omega = \omega + i\Omega$, where Ω determines the CWs' temporal damping. These roots become purely imaginary ($\omega = 0$) for

$$\gamma\rho/(4\eta^2 k) < 0.145, \quad (2)$$

indicating that propagating CWs are prohibited [28].

The actual thermal population of the hydrodynamic modes is given by Jäckle and Kawasaki's (JK) [27] linear

response theory, yielding the CW (ripplon) spectrum

$$S(k, \omega) = -[2k_B Tk/(\rho\omega)]\text{Im } D(k, \omega)/|D(k, \omega)|^2. \quad (3)$$

For negligible damping, Eq. (3) yields sharp Brillouin (Stokes and anti-Stokes) peaks, centered at $\omega = \pm(gk + \gamma k^3/\rho)^{1/2}$. For strongly overdamped CWs, the spectrum is well approximated by a single Lorentzian, centered at $\omega = 0$. Neither limit applies here, as revealed by substitution of the appropriate values into Eq. (2). Thus, $S(k, \omega)$ must be Fourier transformed numerically to yield $C(k, \tau)$ [21]. $C(k, \tau)$ is real since $S(k, \omega) = S(k, -\omega)$. Measured $G(q_x, \tau)$ exhibits both heterodyne and homodyne contributions in varying proportions. These originate, respectively, in wave mixing in the presence, or absence, of a reference beam—the wings of the specular reflection [24]. Explicitly accounting theoretically for both contributions yields

$$G(q_x, \tau) = A\phi\tilde{C}(q_x, \tau) + |A\tilde{C}(q_x, \tau)|^2. \quad (4)$$

$\tilde{C}(q_x, \tau) = \int C(q', \tau)\Theta(q_y - q_y')dq_y'$, where $\Theta(q)$ is the experimental (rectangular) resolution function [29] and $q' = [q_x^2 + (q_y')^2]^{1/2}$.

Equation (4) includes only two unknowns: A, the overall intensity factor, and ϕ, the homodyne to heterodyne contribution ratio. Using those as fit variables, all XPCS curves measured for 303 K $\leq T \leq$ 413 K and 13 mm$^{-1} \leq q_x \leq$ 78 mm^{-1} could be well fitted. Figure 1 (lines) demonstrates the excellent fits, obtained using independently measured γ, η, and ρ [31].

The fitted A and ϕ were used to calculate the *experimental* CWs' spectra from the experimental $G_{\exp}(q_x, \tau)$ curves in Fig. 1, by inverting Eq. (4),

$$\tilde{C}(q_x, \tau) = \{[A^2\phi^2 + 4A^2 G_{\exp}(q_x, \tau)]^{1/2} - A\phi\}/(2A^2), \quad (5)$$

noting that $\tilde{C}(q_x, \tau)$ is real, and that only the positive root in Eq. (5) is physical. The Fourier transform of $\tilde{C}(q_x, \tau)$, $\tilde{S}(q_x, \omega)$, yields the resolution-modified *experimental* CW spectrum,

$$\tilde{S}(q_x, \omega) = \int S(q', \omega)\Theta(q_y - q_y')dq_y', \quad (6)$$

in Fig. 2 (symbols). For low damping (i.e., low q_x and high T), $\tilde{S}(q_x, \omega)$ exhibits well-separated inelastic-scattering Stokes and anti-Stokes Brillouin peaks, corresponding to propagating CWs. As η increases, the two peaks merge to a single peak centered at $\omega = 0$. Here the CWs are overdamped, and the scattering is quasielastic, since energy transfer to propagating CWs is prohibited [32]. Substitution of Eq. (3) into Eq. (6) yields the *theoretical* CW spectra (Fig. 2, lines). The good agreement, without any adjustable parameters, is evident. The only earlier attempt at a similar analysis [19], addressed only pure heterodyne curves, neglected resolution, and treated γ and η as additional fit parameters. These, and the poorer data yielded significant deviations between theory and experiment.

A and ϕ are related to the scattered, I_s, and the reference, I_r, intensities. Discarding τ-independent background terms, the normalized time-averaged ($\langle\cdots\rangle$) intensity autocor-
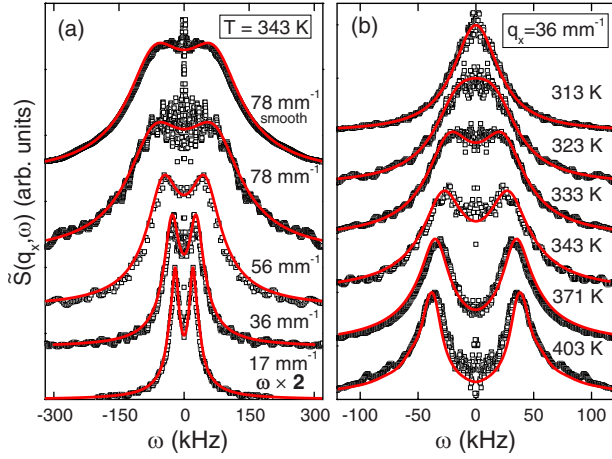
FIG. 2. (Color online) Experimental (symbols) and theoretical (lines) dynamic structure factors, for the listed q_x (a) and T (b). The top curve in (a) is a pre-Fourier-transform-smoothed version of the curve below it. The ω axis for $q_x = 17$ mm^{-1} is twofold expanded for clarity.

FIG. 3. (a) Time-averaged scattered intensities I_s (symbols). Line: q_x^{-2} law. (b) Measured Brillouin peak positions (solid symbols) and the theoretical decay of ω calculated from hydrodynamics near T_c^{LL} (solid line) and from linear response theory near T_c^{JK} (open symbols) for the listed q_x vs *relative T*. Dashed lines: $(T - T_c)^{1/2}$ power laws. Inset: same as (b) for $q_x = 24$ mm^{-1} vs *absolute T*.

relation signal is $G_{\exp}(q,\tau) \equiv \langle I(q,t)I(q,t+\tau) \rangle / \langle I(q,t) \rangle^2 = [2I_sI_r g^{(1)}(\tau) + I_s^2 g^{(2)}(\tau)]/(I_r+I_s)^2$ [23]. $g^{(1)}(\tau)$ and $g^{(2)}(\tau)$ are the first- and second-order correlation functions of the scattered field. Since $g^{(1)}(\tau) = I_s^{-1} C(q,\tau)$ and $g^{(2)}(\tau) = 1 + |g^{(1)}(\tau)|^2$, we obtain

$$G_{\exp}(q,\tau) = [2I_r C(q,\tau) + |C(q,\tau)|^2]/(I_r+I_s)^2. \quad (7)$$

Neglecting resolution, $C(q,\tau) = \tilde{C}(q,\tau)$. Equating the prefactors in Eqs. (7) and (4) yields $I_r = \phi/(2A)$ and $I_s = (2-\phi)/(2A)$, which can now be calculated from the fitted A and ϕ. $I_r(q_x)$ shows no consistent trend vs q_x beyond a statistical scatter, and a random time variation. $I_s(q_x)$, however, follows, within some scatter, the q_x^{-2} power law [Fig. 3(a)], predicted and observed for the time-averaged diffuse CW scattering [13]. This further validates our analysis.

Interestingly, for our γ, η, and ρ, the *theoretical* critical temperature T_c^{JK}, where the inelastic double-peak structure merges into a single quasielastic scattering peak, is found to be, for all k, ~ 10 K higher than T_c^{LL}, the *theoretical* hydrodynamic critical temperature of Eq. (2) [Fig. 3(b), inset]. This can be traced to the critical damping conditions, $\eta(T_c) \approx (\mu \gamma \rho/k)^{1/2}$, where the hydrodynamic dispersion relation [Eq. (2)] yields $\mu = 1.7$, while the $S(k,\omega)$ spectra [19] yield $\mu = 0.8$. The *measured* $S(k,\omega)$ are indeed observed to become completely overdamped at $T_c^{JK} \gg T_c^{LL}$, in agreement with the linear response theory [27]. This is easily rationalized: the dispersion relation merely states that ripplon propagation is *hydrodynamically* allowed for $T > T_c^{LL}$, however, *thermodynamically*, the thermal population of these modes at $T < T_c^{JK}$ is so small that only quasielastic scattering is observed. Put differently, the short lifetime of the ripplons for $T < T_c^{JK}$ broadens the off-center Brillouin peaks of $S(k,\omega)$, so that $S(k,\omega=0)$ becomes larger than the Brillouin peaks, $S(k,\omega=\pm\omega_p)$: only the quasielastic scattering ($\omega=0$) is now allowed. The same effect is observed for the much simpler case of a damped pendulum as a damping-induced lowering
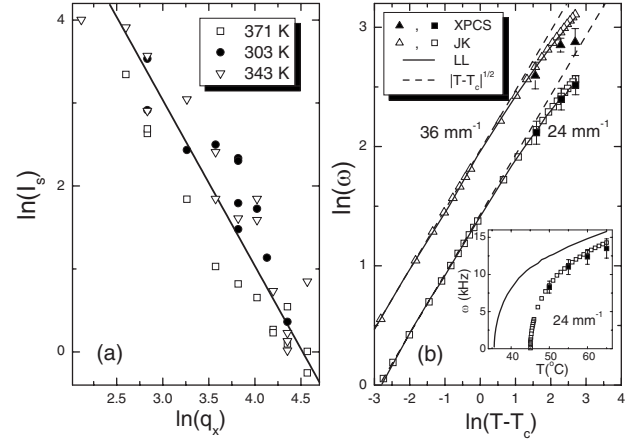
of the actual resonance frequency below the eigenfrequency [33].

Figure 3(b) shows the propagating CWs' ω, calculated from the dispersion relation [Eq. (1)] (lines) and peak positions ω_p of $S(k,\omega)$ (open symbols). Both exhibit the same power-law behavior, with a $1/2$ critical exponent, even though the corresponding critical temperatures (T_c^{LL} and T_c^{JK}, respectively) differ by ~ 10 K (inset). While available intensities prohibit measurements very close to T_c, the measured ω_p (closed symbols) follow closely the linear response theory [27], both close to [main Fig. 3(b)] and far from (inset) criticality.

The critical exponent $1/2$ is obtained in the linear response theory by noting that near criticality $\omega_p \approx (2/3)\text{Re}(\gamma k^3/\rho - 5\varepsilon^2/4)^{1/2}$ [19]. Neglecting ρ's weak T dependence, $\nu(T)$ follows the exponential form of $\eta(T)$. Nothing special happens in the bulk at T_c^{JK}, which is a transition in the *surface* dynamics. Thus, expanding $\nu(T)$ in $t = T - T_c^{JK}$, $\nu(T \to T_c^{JK}) = \nu(T_c^{JK}) - \zeta t + \cdots$, substituting in ω_p above, and keeping terms up to linear,

$$\omega_p(T) = \text{Re}[\omega_p^2(T_c^{JK}) + (10/9)k^4 \nu(T_c^{JK})\zeta t]^{1/2}. \quad (8)$$

Since no inelastic scattering occurs at T_c^{JK}, $\omega_p(T \to T_c^{JK}) \to 0$, and the $t^{1/2}$ power law is obtained.

In conclusion, the T and k dependences of the CW spectrum of [bmim][BF$_4$] have been determined by XPCS. We demonstrate that the measured $G(q_x,\tau)$ can be accurately analyzed by a direct application of the linear response theory, using only two fit parameters: the overall intensity and the homodyne-to-heterodyne intensity ratio. The fits allow calculations of the *experimental* CWs spectra, which exhibit a transition from propagating to overdamped modes. Brillouin scattering by the propagating modes is extinguished ~ 10 K *above* the hydrodynamically predicted critical temperature where the CWs become overdamped by viscosity. Nevertheless, ω still approaches both temperatures with the same $1/2$

power law. The good theory-experiment agreement, obtained using independently measured γ, and bulk η and ρ, implies negligible influence of the [bmim][BF$_4$] dense surface layer [8]. This is perhaps not too surprising, since assuming the (unknown) dilational modulus of the layer to equal $\gamma/2$ yields a calculated $\lesssim 10\%$ decrease only in ω_p in our q_x range. This would be difficult to resolve in our experiment. In low-viscosity liquids, the influence of surface layers is clearly observed [15,17]. The dipole layer of density ~ 2 nC/m found by DLS for [bmim][PF$_6$] [18] should have yielded here, e.g., a well-observable 40% decrease in ω_p at $q_x = 36$ mm^{-1}, and a conversion of the clearly propagating CWs at $q_x = 56$ mm^{-1} [see Figs. 1(a) and 2(a)] to overdamped CWs. These effects are not observed, indicating a dipole surface layer, if it exists, with fivefold (or more) lower dipole density. XPCS measurements for additional RTILs, e.g., [bmim][PF$_6$], are required to better elucidate the surface dynamics of RTILs.

[1] P. Walden, Bull. Acad. Imper. Sci. **22**, 405 (1914).

[2] T. Welton, Chem. Rev. (Washington, D.C.) **99**, 2071 (1999); P. Wasserscheid and W. Keim, Angew. Chem. **39**, 3772 (2002).

[3] M. J. Earle, J. M. S. S. Esperança, M. A. Gilea, J. N. C. Lopes, L. P. N. Rebelo, J. W. Magee, K. R. Seddon, and J. A. Widegren, Nature (London) **439**, 831 (2006).

[4] U. Bach, D. Lupo, P. Comte, J. E. Moser, F. Weissörtel, J. Salbeck, H. Spreitzer, and M. Grätzel, Nature (London) **395**, 583 (1998); P. Wang *et al.*, J. Am. Chem. Soc. **125**, 1116 (2003).

[5] E. F. Borra, O. Seddiki, R. Angel, D. Eisenstein, P. Hickson, K. R. Seddon, and S. P. Worden, Nature (London) **447**, 979 (2007).

[6] L. Crowhurst, N. L. Lancaster, J. M. P. Arlandis, and T. Welton, J. Am. Chem. Soc. **126**, 11549 (2004); C. Pinilla, M. G. Del Popolo, J. Kohanoff, and R. M. Lynden-Bell, J. Phys. Chem. B **111**, 4877 (2007).

[7] R. M. Lynden-Bell and M. Del Pópolo, Phys. Chem. Chem. Phys. **8**, 949 (2006).

[8] E. Sloutskin, B. M. Ocko, L. Tamam, I. Kuzmenko, T. Gog, and M. Deutsch, J. Am. Chem. Soc. **127**, 7796 (2005).

[9] W. Lu *et al.*, Science **297**, 983 (2002); W. Xu and C. A. Angell, *ibid.* **302**, 422 (2003); C. S. Santos, S. Rivera-Rubero, S. Dibrov, and S. Baldelli, J. Phys. Chem. C **111**, 7682 (2007).

[10] D. Tomida, A. Kumagai, K. Qiao, and C. Yokohama, Int. J. Thermophys. **27**, 39 (2006).

[11] T. Iimori, T. Iwahashi, K. Kanai, K. Seki, J. Sung, D. Kim, H. Hamaguchi, and Y. Ouchi, J. Phys. Chem. B **111**, 4860 (2007); R. D. Rogers and K. R. Seddon, Science **302**, 792 (2003).

[12] J. Bowers, M. C. Vergara-Gutierrez, and J. R. P. Webster, Langmuir **20**, 309 (2004).

[13] A. Braslau, P. S. Pershan, G. Swislow, B. M. Ocko, and J. Als-Nielsen, Phys. Rev. A **38**, 2457 (1988); B. M. Ocko, X. Z. Wu, E. B. Sirota, S. K. Sinha, and M. Deutsch, Phys. Rev. Lett. **72**, 242 (1994)

[14] D. G. A. L. Aarts, M. Schmidt, and H. N. W. Lekkerkerker, Science **304**, 5672 (2004).

[15] R. C. McGivern and J. C. Earnshaw, Langmuir **5**, 545 (1989).

[16] V. G. Levich, *Physicochemical Hydrodynamics* (Prentice-Hall, Englewood Cliffs, NJ, 1962); E. H. Lucassen-Reynders and J. Lucassen, Adv. Colloid Interface Sci. **2**, 347 (1969).

[17] P. Huber, V. P. Soprunyuk, J. P. Embs, C. Wagner, M. Deutsch, and S. Kumar, Phys. Rev. Lett. **94**, 184504 (2005).

[18] V. Halka, R. Tsekov, and W. Freyland, Phys. Chem. Chem. Phys. **7**, 2038 (2005) V. Halka, R. Tsekov, I. Mechdiev, and W. Freyland, Z. Phys. Chem. **221**, 549 (2007).

[19] A. Madsen, T. Seydel, M. Sprung, C. Gutt, M. Tolan, and G. Grübel, Phys. Rev. Lett. **92**, 096104 (2004).

[20] C. Gutt, T. Ghaderi, V. Chamard, A. Madsen, T. Seydel, M. Tolan, M. Sprung, G. Grübel, and S. K. Sinha, Phys. Rev. Lett. **91**, 076104 (2003); **91**, 179902 (2003).

[21] T. Ghaderi, Ph.D. thesis, Dotrmund University, 2006 (unpublished); S. K. Sinha, M. Tolan, and A. Gibaud, Phys. Rev. B **57**, 2740 (1998); M. Tolan, T. Seydel, A. Madsen, G. Grbel, W. Press, and S. K. Sinha, Appl. Surf. Sci. **182**, 236 (2001).

[22] T. Seydel, A. Madsen, M. Sprung, M. Tolan, G. Grübel, and W. Press, Rev. Sci. Instrum. **74**, 4033 (2003); T. Seydel, A. Madsen, M. Tolan, G. Grubel, and W. Press, Phys. Rev. B **63**, 073409 (2001).

[23] J. C. Earnshaw, Appl. Opt. **36**, 7583 (1997).

[24] I. Sikharulidze, I. P. Dolbnya, A. Madsen, and W. H. de Jeu, Opt. Commun. **247**, 111 (2005); W. H. de Jeu, A. Madsen, I. Sikharulidze, and S. Sprunt, Physica B **357**, 39 (2005).

[25] J. C. Earnshaw, Nature (London) **292**, 138 (1981).

[26] L. D. Landau and E. M. Lifshitz, *Fluid Mechanics*, 2nd ed. (Oxford University Press, Oxford, 2000).

[27] J. Jäckle, J. Phys.: Condens. Matter **10**, 7121 (1998); J. Jäckle and K. Kawasaki, *ibid.* **7**, 4351 (1995).

[28] M. A. Bouchiat and D. Langevin, C.R. Seances Acad. Sci., Ser. A **272**, 1357 (1971).

[29] The detector's finite spatial window prohibits resolving intensity autocorrelations at the same angle from cross correlations at different angles within the window. No theoretical treatment of this effect is currently available [21]. Thus, we use Eq. (4), shown here to provide good agreement with experiment.

[30] J. Jacquemin, P. Husson, A. A. H. Padua, and V. Majer, Green Chem. **8**, 172 (2006).

[31] $\gamma(T) = 65.26 - 7.04 \times 10^{-2}T$ mN/m [8], $\eta(T) = 0.0933 \times \exp[937/(T-164)]$ cP [10], and $\rho(T) = 1.219 - 7.17 \times 10^{-4}(T-273.16)$ g/cc [30].

[32] The sharp $\omega = 0$ peaks in Fig. 2 are numerical artifacts due to the finite accuracy in the background subtraction. So are the short-period oscillations on the tails of $\tilde{S}(q_x, \omega)$, arising from Fourier transforming numerically noisy measured curves. Pre-transform smoothing cures this artifact. See the top two curves in Fig. 2(a).

[33] T. C. Lubensky and P. M. Chaikin, *Principles Of Condensed Matter Physics* (Cambridge University Press, New York, 2000).